

# EXPERIMENTAL INVESTIGATION OF UNSTEADINESS ASSOCIATED WITH FILM COOLING FLOW EJECTION FROM THE VANE PRESSURE SIDE

*G. Barigozzi<sup>1</sup>, S. Ravelli<sup>1</sup>, A. Armellini<sup>2</sup>, C. Mucignat<sup>2</sup>, L. Casarsa<sup>2</sup>*

<sup>1</sup> Department of Industrial Engineering – University of Bergamo –Dalmine (BG) - Italy - E mail:  
giovanna.barigozzi@unibg.it, silvia.ravelli@unibg.it

<sup>2</sup> Department of Electric, Management and Mechanical Engineering – University of Udine –Udine -  
Italy - E mail: alessandro.armellini@uniud.it, claudio.mucignat@uniud.it, luca.casarsa@uniud.it

## ABSTRACT

The thermal performance of a gas turbine airfoil with a cooled pressure side and a trailing edge cutback is investigated and discussed in relationship with the unsteady behavior of coolant injection. The focus is on the pressure side coolant injection through discrete holes. The cascade was tested at a low exit Mach number of 0.2 varying the coolant to mainstream mass flow ratio. Laser Doppler Velocimetry (LDV) and high speed flow visualizations were used to investigate the unsteady mixing process taking place between coolant and main flow downstream of the holes. This behavior was correlated with the film cooling effectiveness distributions. In the first row, hairpin clockwise rotating vortices and counterclockwise shear layer vortices were observed, depending on the coolant to mainstream velocity ratio. The second row turned out to be characterized by a lower velocity ratio and lower turbulent activity, consistently with the higher thermal protection observed also at high injection rates.

## NOMENCLATURE

$c$	blade chord
$D$	hole diameter
$f$	frequency
$H$	blade height
$H_{12}$	shape factor
$m$	mass flow rate
$M$	Mach number
$MFR = m_c/m_e$	coolant to mainstream mass flow ratio
$n$	direction normal to the wall
$Re_{2,is} = U_{2,is}c/\nu$	isentropic outlet Reynolds number
$s$	blade pitch, direction tangent to the vane surface
$St = fD/U_c$	Strouhal number
$U, V$	velocity components (parallel and normal to the vane surface)

$VR$	velocity ratio
$X, Y, Z$	cascade coordinate system
$\beta$	flow angle (tangential direction)
$\delta$	boundary layer thickness
$\eta = (T_{aw} - T_{\infty})/(T_c - T_{\infty})$	film cooling effectiveness

## Subscripts

$1$	inlet
$2$	exit
$av$	laterally averaged
$ax$	in axial direction
$c$	cooling flow
$e$	free stream
$is$	isentropic condition
$hole$	related to the holes

## Superscripts

$'$	RMS
-----	-----

## INTRODUCTION

Improvement of gas turbines performance through the increase in turbine inlet temperature requires an adequate thermal protection of the high pressure turbine stage. In particular the flow path surfaces of first stage turbine vanes and platform need to be shielded from the hot mainstream gas exiting the combustor. Usually a combination of internal convective cooling and external film cooling is employed to assure the integrity of end walls and airfoils, especially in the most difficult regions to be cooled, such as the leading and trailing edge. To allow turbine vanes and blades to sustain such high thermal loads a very efficient cooling system is required; this means to search for film cooling maximum effectiveness in order to limit the air consumption. So, accurate information on the interaction of coolant injection with boundary layers developing on the airfoils is required to optimise the cooling design, from both the aerodynamic and thermal point of view.

An impressive number of investigations have been carried out in the past to analyse all the aspects involved in the film cooling process (Han et al (2000)). Many experiments have been carried out, mostly on film cooled simplified models as flat plates, showing the influence of various parameters, e.g. hole geometry, blowing, momentum and density ratios and free-stream turbulence. These studies allowed to examine the near hole exit flow field, dominated by the presence of vortical structures, the so called kidney vortex pairs. Several CFD studies on film cooling are also available in the published journals. The steady RANS approach usually fails to capture the jet lateral spreading and mixing process, resulting in an over prediction of the film cooling effectiveness values going downstream. The reason why RANS simulations fail to predict the film cooling behaviour can be related to the fact that jet to mainstream interaction is an unsteady and highly anisotropic process. Much better prediction capability can be obtained by using simulation approaches like DES or LES (Tyagi and Acharya (2003), Roy et al. (2003)). They capture the unsteady jet to mainstream mixing process which plays a dominant role in the airfoil surface thermal protection, for a specific cooling scheme. The unsteady CFD approach in turns requires detailed experimental data to be fully validated. This is surely challenging as the time varying flow behaviour or at least the turbulence characteristics are much difficult to measure than the mean flow characteristics, especially in a cascade environment. In fact, only little information is available on the unsteady jet to mainstream interaction in the near hole exit region. Pietrzyk et al. (1989,1990), Sinha et al. (1991) and Thole et al. (1996) investigated the mean and turbulent flow field structure both downstream of cylindrical and fan shaped holes on flat plate models, by varying blowing and density ratios and simulating multiple row injection. Barigozzi et al. (2003) tested a full coverage film cooled vane cascade to measure the mean and turbulent flow field characteristics in the rear pressure and suction side, downstream of cylindrical holes, for variable injection conditions and inlet turbulence intensity levels. But at author's knowledge, only Fawcett et al. (2010, 2011) experimentally documented the unsteady behaviour of coolant jets on a low speed blade cascade with a single row injection on the front pressure side. PIV data and high speed flow visualizations confirmed the presence of coherent unsteadiness consisting in vortices located in the shear layer between the jet and the mainstream for a blowing ratio of 2.0 and of hairpin vortices for a lower blowing ratio of 0.5. The vortices located in the shear layer were thought to result from a Kelvin-Helmholtz breakdown, with the velocity gradient across the shear layer being the driving factor. Moreover, these vortices and the hairpin vortices rotate in opposite direction.

The present paper is aimed at verifying this phenomena under geometrical and flow conditions closer to the real applications and at deepening Fawcett et al. study by combining thermal and aerodynamic measurements. A cooling configuration with a pressure side trailing edge cutback and two cooling rows placed upstream of the cutback was experimentally investigated. Experiments were conducted in a subsonic linear cascade with high pressure nozzle guide vanes. All tests were performed at low speed, with an exit Mach number  $M_{2is}$  of 0.2, by varying the coolant to mainstream mass flow ratio up to about 3.0%. Boundary layer measurements downstream both injection rows and high speed flow visualizations were performed to fully describe, from both a

time-mean and an unsteady point of view, the complex coolant to mainstream mixing process for variable injection conditions, also in relationship with film cooling effectiveness data. Other aerodynamic and thermal results for the same configuration can be found in a previous paper (Barigozzi et al. (2012)). Moreover, a similar investigation is documented in Barigozzi et al. (2012) with a focus on the cutback region.

## EXPERIMENTAL SETUP

### The wind tunnel and the cascade model

Tests were performed in the subsonic wind tunnel for linear cascades at the Turbomachinery Laboratory of Bergamo University. This is a continuously operating, suction-type wind tunnel (Fig. 1). The side walls are constructed of Plexiglas for optical accessibility. A six-bladed linear turbine cascade was investigated. Details of cascade geometry are reported in Table 1 and Fig. 2. The vane profile imposes a design flow turning of  $70^\circ$ . The vane is characterized by a Zweifel coefficient of 1.18, indicating a highly loaded vane.

The trailing edge of the three central vanes is equipped with two staggered rows of cylindrical holes and a cutback, all located on the pressure side. As shown in Fig. 3, the first row is composed of 23 cooling holes and it is located at  $X/c_{ax} = 0.52$ . The second row is composed of 24 holes and it is located at  $X/c_{ax} = 0.64$ . Within each row, the hole-to-hole pitch is  $2.76D$ . The diameter of the cooling holes  $D$  is 1.05 mm. The holes are angled at  $30^\circ$  to the surface. Holes and cutback are spread over 70% of the vane height. The cutback starts at  $X/c_{ax} = 0.72$  and it consists of 8 equally spaced rectangular slots. In order to increase the stiffness of the thin trailing edge and to enhance the internal heat transfer, an arrangement of rib arrays was adopted. Coolant air is supplied by a radial fan through a plenum chamber, connected to the vanes by flexible ducts.



Fig. 1: View of the wind tunnel.

Table 1: Cascade geometry and operating conditions.

$c = 142.1 \text{ mm}$	$\beta_2 = 20^\circ$
$s/c = 1.04$	$M_{2is} = 0.2$
$H = 98 \text{ mm}$	$Re_{2is} = 6.5 \cdot 10^5$
$H/c = 0.69$	$Tu_1 = 1.7 \%$
$\beta_1 = 90^\circ$	$MFR = 0.0 - 2.9 \%$

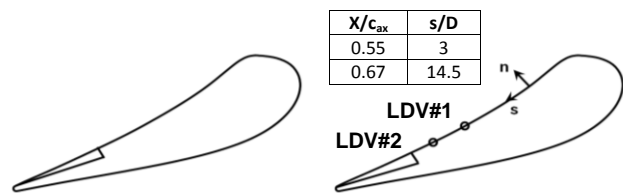
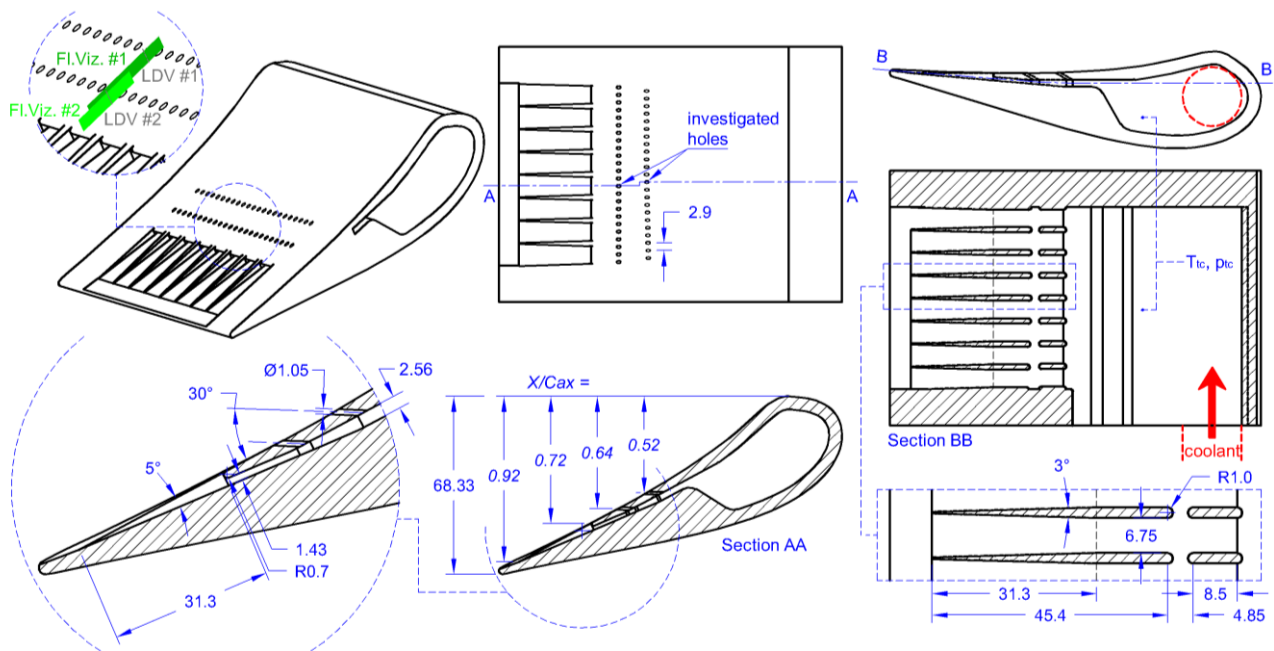


Fig. 2: Vane cascade geometry and LDV measurements location.

### Testing Conditions and Instrumentation

The cascade was tested at a constant exit Mach number  $M_{2is} = 0.2$ , corresponding to a  $Re_{2is}$  of  $6.5 \cdot 10^5$  and at a low inlet turbulence intensity level  $Tu_1 = 1.7\%$ . This operating condition was chosen because it allows to get good quality high speed flow visualizations in the near hole exit region. In fact, at higher Mach number wind tunnel vibrations would make the data acquisition more challenging; a higher turbulence intensity would instead have required to install a turbulence generator in the tunnel inlet section making illumination of the investigated region practically

impossible. Finally, even if the vane was designed to work at  $M_{2is} = 0.6$  and  $Re_{2is} = 10^7$ , compressibility effects are quite limited, making the actual operating conditions not so different from the real one, especially upstream of the cutback. The main difference will rely on the much higher acceleration that a high Mach and Reynolds number operating condition imposes along the rear pressure side. Conversely, the region interested by hole injection would not be strongly influenced by a change in Mach and Reynolds numbers. Concerning the turbulence intensity level, much higher turbulence levels characterize the gas flow coming from the combustion chamber. Radomski and Thole (2002) have shown that an increase in  $Tu_1$  from 0.6% up to about 19% is only responsible for increased velocity fluctuations and wall shear stress along the pressure side, with the boundary layer still showing a laminar like behavior. This was due to the high acceleration that prevented transition. But when the vane pressure side is cooled, boundary layer behavior is completely dominated by coolant injection, making the influence of  $Tu_1$  of minor relevance.



**Fig. 3: Trailing edge cooling geometry (dimensions in mm).**

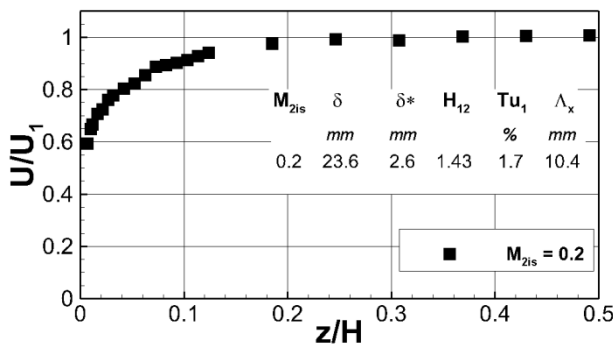


**Fig. 4: Inlet boundary layer profile ( $X/c_{ax} = -1.6$ ).**

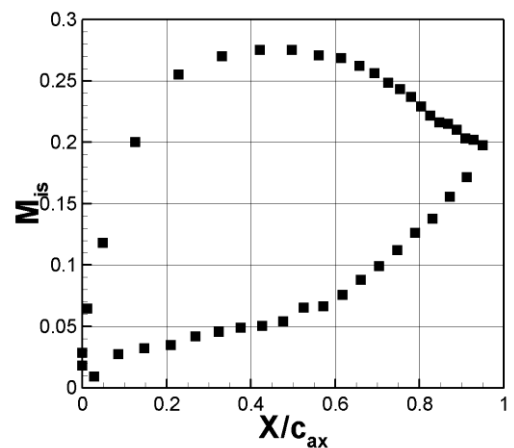


**Fig. 5: Blade load (solid vane).**

Cascade operating conditions (Table 1) were controlled by monitoring the inlet total and static pressure and the exit static pressure ( $X/c_{ax} = 1.45$ ). Inlet total pressure and static pressure were measured by a three-hole probe in the admission section, about  $1.6c_{ax}$  upstream of the cascade inlet plane. In the same location the inlet boundary layer and

the turbulence intensity were also measured using a flattened Pitot tube and a hot-wire probe (Fig. 4). The measured mid span solid airfoil  $M_{is}$  profile is shown in Fig. 5. The blunt leading edge is responsible for the strong acceleration up to almost  $0.5c_{ax}$  along the suction side, followed by a strong diffusion up to the trailing edge. The pressure side is instead characterized by a continuous acceleration up to the trailing edge, which is especially relevant downstream of  $X/c_{ax} = 0.6$ .

Overall mass flow ratios up to about 3% were studied. Injection conditions were controlled through a continuous monitoring of the global coolant to mainstream mass flow ratio  $MFR$  and the coolant total pressure in the three vane feeding chambers (secondary air is at room temperature). The injected mass flow was measured by an orifice device. A HP 3852A D.A.C.U. unit (12 bit resolution) was used to acquire all pressure ( $\pm 100$  mV range) and temperature ( $\pm 0.1^\circ\text{C}$ ) data. The uncertainty in the  $MFR$  value was computed according to international standards for orifice devices (EN ISO 5167-2:2003(E)).  $\delta MFR$  resulted to be  $\pm 0.04\%$  at a value of  $MFR = 0.5\%$  and  $\pm 0.05\%$  at a value of  $MFR = 2.8\%$ .

A 2D LDV system was used to study the boundary layer behaviour just downstream of both hole locations ( $\sim 1$  mm, corresponding to 3D downstream of the holes leading edge, where the hole coordinate system origin is located, see Figures 2 and 3). The light source was a 300 mW Ar+ laser. A 200 mm focal length front lens allowed to measure a volume 0.06 mm in diameter and 0.6 mm in length. Two Burst Spectrum Analyzers were used to process the signals coming from the photomultipliers. All measurements were carried out acquiring 40000 burst signals at each location in coincidence mode. Sawdust smoke was used to seed the flows, both main stream and coolant. The high number of acquired signals assured statistically accurate averages: based on a 95% confidence level, uncertainties of  $\pm 0.41\%$  and  $\pm 0.7\%$  for mean and RMS values, respectively, have been obtained for a turbulence intensity level of 42%. Location of boundary layer traverses is shown in Fig. 2 and 3. All traverses extend 2 mm perpendicularly to the vane surface and are located on the holes centreline closest to the vane midspan. Each traverse was divided into 18 measuring points whose spacing was reduced down to 0.03 mm approaching the wall. All collected data have been corrected for velocity bias and error related to velocity gradients (Karpuk and Tiedermann (1976)). A computer controlled three axis traversing system driven by stepping motors assures a probe minimum linear displacement of 10  $\mu\text{m}$ . The probe can also be continuously rotated around all three axis, thus making it possible to approach the vane surface everywhere. The probe was oriented in such a way to directly measure the parallel (U) and the normal (V) velocity components, with respect to the vane surface.

Flow visualizations were performed on a blade-to-blade plane located at the mid span of each hole where the LDV measurements were performed. The visualizations were obtained using the components of a PIV measurement chain which comprises a 125 mJ double cavity Nd:Yag laser and a 12-bit cooled CCD camera (PCO Sensiscam) with a resolution of 1024x1280 pixels and equipped with Nikkor lenses. The camera was tilted with respect to the laser sheet in order to maximize the field of view towards the vane surface. Consequently it was mounted on a two-axes Scheimpflug adapter to get a good image focusing over the viewing plane. A good image contrast was obtained by seeding only the coolant flow with high particle density. A target made of an orthogonal grid of black dots on white background with a spacing of 1x1 mm was used to perform image positioning and dewarping, i.e. to perform the perspective correction. Consequently, thanks to this calibration procedure, the flow visualization images are correctly scaled and positioned with respect to the vane reference frame.

## RESULTS AND DISCUSSION

In the following, injection conditions will be first discussed in order to provide a relationship between the usual overall coolant parameter  $MFR$  and local injection conditions, typically defined by the velocity ratio  $VR$ , i.e. the ratio between the bulk coolant velocity and the mainstream velocity at the holes exit location. Laterally averaged film cooling effectiveness data will also be introduced, to give the reader an overview of the thermal protection performance of the cooling scheme. Then

instantaneous images of the cooling flow coming from the first row of holes and LDV boundary layer profiles, collected at a constant  $M_{2is}$  of 0.2 for variable injection conditions, will be presented and discussed in relation with laterally averaged film cooling effectiveness data. The same analysis is finally repeated for the second row of holes.

### Holes injection conditions

The injection system was characterized through a set of tests with both holes and cutback blowing, by varying the coolant to mainstream mass flow ratio  $MFR$ . The same tests were repeated with only the cutback blowing. These data were used to define the mass flow sharing between holes and cutback which is necessary to calculate the holes coolant to mainstream mass flow rate ratio  $MFR_{hole}$ . Table 2 summarizes the correspondence between overall and holes  $MFR$  values. Please note that a  $MFR$  lower than 1.0% gave rise to flow ingestion through the rows of holes, as hole exit pressure was higher than coolant total pressure measured inside the vane cavity. An overall mass flow rate for all the holes belonging to both rows #1 and #2 was calculated, since it was practically impossible to perform tests without the cutback blowing. Furthermore the mass flow through a single row is too small compared to the whole system blowing. From these data the coolant exit velocity was computed assuming incompressible flow condition and an even mass flow sharing between all the holes belonging to the two rows:

$$U_c = \frac{4m_c}{\rho N_{hole} \pi D^2} \quad (1)$$

The hole Reynolds number values reported in Table 2 are based on these coolant velocity values. The velocity ratio  $VR$  for each row was calculated by dividing this unique value by the freestream velocity at hole exit  $U_e$ , with the latter derived from Fig. 5 data, assuming that coolant injection does not significantly alter the solid vane load profile:

$$VR_{\#row} = U_c / U_{e,\#row} \quad (2)$$

This assumption was confirmed by Puddu et al. (2011) who tested the same cooled vane geometry. Figure 6 reports the calculated  $VR$  values plotted against  $MFR_{hole}$  for both rows of holes (black symbols). The higher  $VR$  values of row #1 have to be related to the lower free stream velocity at this location. A strong uncertainty in the  $VR$  values comes from the assumption that the same amount of coolant is discharged by each row. Boundary layer traverses presented in the following sections were used to verify this assumption. From mean velocity profiles the peak value was extracted whenever a clear identification of the coolant jet was possible, i.e. for large injection conditions. The hollow symbols in Fig. 6 indicate the  $VR$  values computed using the LDV peak velocity. As clearly shown, the LDV data indicate higher peak values for row #1 and lower for row #2 with respect to the original approach. Bearing in mind that the original approach makes use of a mass averaged coolant velocity rather than of a peak jet velocity, it can be in any case concluded that the coolant mass flow is actually unevenly shared between the two rows, with row #1 surely discharging a

**Table 2: Injection conditions (LDV traverses).**

$MFR$	$MFR_{hole}$	$Re$
1.05	0.18	575
1.24	0.27	882
1.76	0.53	1707
2.25	0.68	2192
2.89	0.87	2825

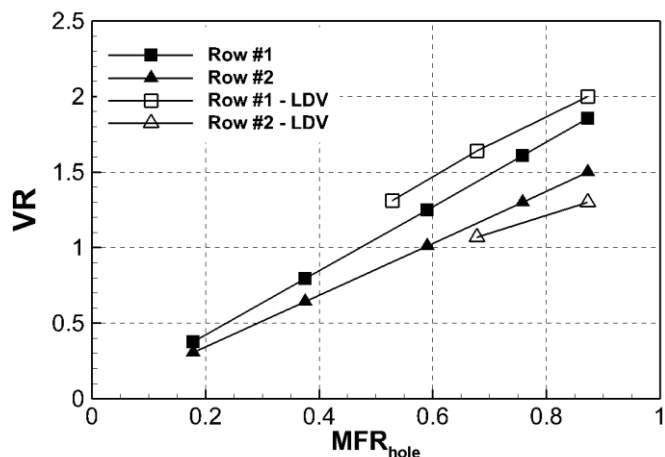


**Fig. 6. VR versus  $MFR_{hole}$ .**

larger amount of coolant. The reduced blowing for row#2 is due to the presence of the ribs in the feeding channel. Finally, it is important to put in evidence the  $MFR$  value for which  $VR$  becomes greater than unity: a  $MFR_{hole}$  higher than 0.35 - 0.4 will assure a  $VR$  larger than 1.0 for row #1 (from LDV data extrapolation) while for row #2 a higher  $VR$  value is required, of about 0.6 - 0.7.

### Film cooling effectiveness

Film cooling effectiveness measurements performed on the same cooled vane cascade are available in Barigozzi et al. (2012). Laterally averaged  $\eta$  distributions for variable injection conditions are reported in Fig. 7 as a function of the curvilinear coordinate  $s$  normalized with the hole diameter. Only the region cooled by holes is reported, i.e.  $s/D$  axis extends up to the cutback lip position. The data show different thermal protection capabilities provided by the two rows of holes at different injection conditions. For low values of  $MFR$ , the coolant is ejected only through the cutback slots and no flow exits through the upstream holes, indeed negligible values of thermal effectiveness are reported in Fig. 7 for the  $MFR = 0.8\%$  case. A small increase in  $MFR$  ( $MFR = 1.2\%$  in Fig. 7, corresponding to a  $MFR_{hole}$  of 0.22%) guarantees an effective thermal protection by both rows of cooling holes, with slightly higher values of effectiveness detected downstream of row #2. On the opposite, different behaviors are found at higher blowing ratios: for  $MFR_{hole}$  greater than 0.66% film cooling protection is almost absent downstream of row #1 whilst it is substantial downstream of row #2, although with lower values with respect to the previous case at  $MFR_{hole} = 0.22\%$ . A phenomenological explanation about the different thermal performances of the two rows of cooling jets here commented is provided by the aerodynamic analysis that follows. Figure 8 finally reports the local  $\eta$  values extracted along the central portion of the span, at  $5D$  downstream of row #2 ( $s/D = 19.5$  in Fig. 7). As clearly shown, the jet lateral spreading is maximum at the lowest injection rate, resulting in a quite uniform  $\eta$  distribution at the middle of the span. Much higher variations in  $\eta$  along the span are detected while increasing the  $MFR$ . At the highest injection condition the peak  $\eta$  values start to decrease, indicating a reduction in the thermal coverage levels.

### Aerodynamic characterization of the film cooling jets

#### First cooling row (Row #1).

The results from the LDV measurements are reported in Fig. 9 in terms of profiles of time averaged streamwise velocity component, streamwise and wall normal rms velocities and associated

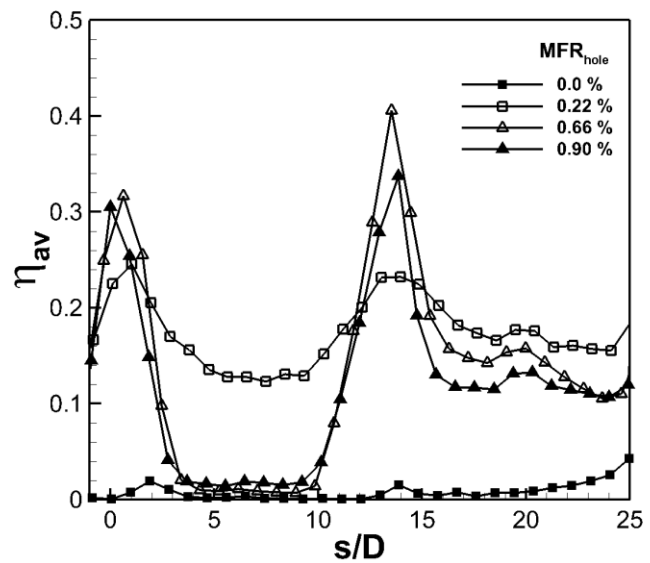


**Fig. 7. Laterally averaged film cooling effectiveness.**

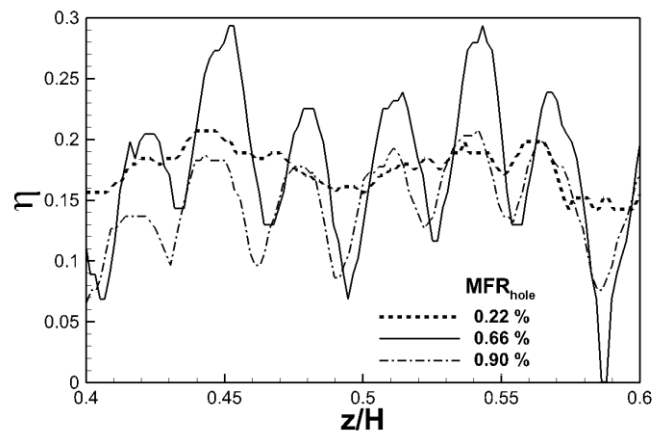


**Fig. 8. Local film cooling effectiveness at  $5D$  ( $s/D = 19.5$ ) downstream of row#2.**

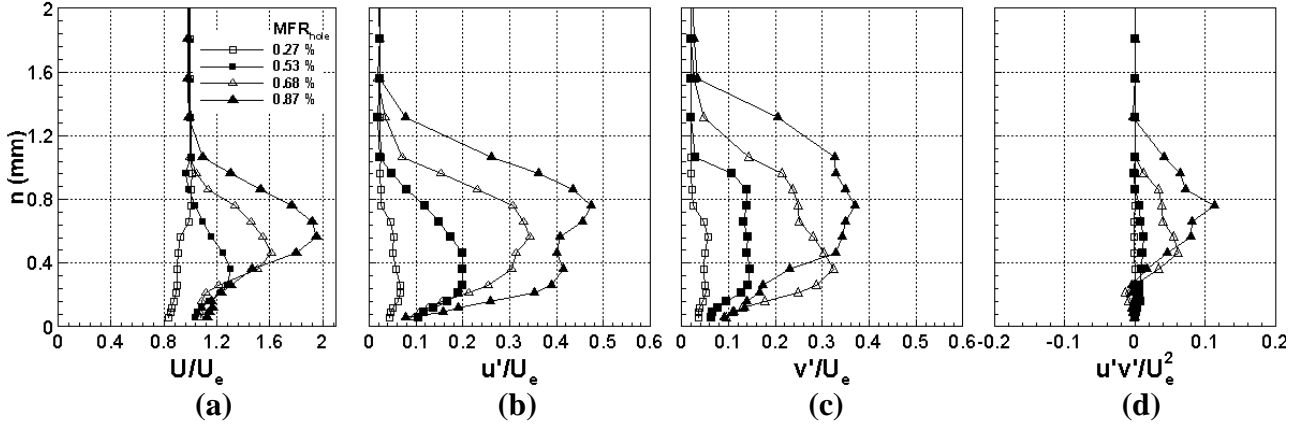


**Fig. 9: Row #1 boundary layer profiles ( $s/D = 3$  - hole centreline).**

shear stress components. The data are normalized with respect to the local free-stream velocity ( $U_e$ ). For low blowing conditions ( $MFR_{hole} = 0.27\%$ ), the velocity profile in Fig. 9a shows that the coolant flow stays close to the vane surface with velocity values always lower than the free stream one. This evidence, associated with the absence of appreciable shear stresses and low velocity fluctuations (Figs. 9b-d), indicates a moderate mixing between coolant and main stream flows that, as reported in Pietrzyk et al. (1989), is normally associated to a  $VR$  slightly lower than 1. When  $MFR_{hole}$  is increased above 0.53%, the streamwise velocity profile is characterized by a remarkable overspeed (up to  $2U_e$  for the highest tested  $MFR_{hole}$  of 0.87%) whose peak is found at increasing elevations with rising injection condition. Consistently with a  $VR$  above one, high turbulent activity is found inside the shear layer between coolant and main stream, with velocity fluctuations as large as 40% of the free stream velocity and a certain degree of anisotropy, especially at the jet boundaries. For  $MFR_{hole} = 0.68\%$  and 0.87%, slightly negative values of shear stresses are found close to the vane surface: it might indicate jet lift-off. Moreover, the high values of velocity fluctuations (see Figs. 9-b,c) measured at increasing distances from the wall for  $MFR_{hole} > 0.53\%$  are an indication of the existence of a strong mixing between coolant and main flow with consequent fast jet spread in the wall-normal direction.

Selected images from the flow visualizations are reported in Fig. 10 and are used to provide a phenomenological explanation of the results above commented about the flow statistics. For the blowing condition at  $MFR_{hole} = 0.18\%$  (Fig. 10a), a confined coolant jet attached to the vane surface is indeed observed. Only far away from the injection point ( $s/D > 10$ ) traces of coherent vortical structures are detected. They appear as clockwise vortices that are the footprints on the image plane of hairpin structures. These latter have been previously shown in the literature, by the Large Eddy Simulation of Tyagi and Acharya (2003) and by the experiments of Fawcett et al. (2011), to be the

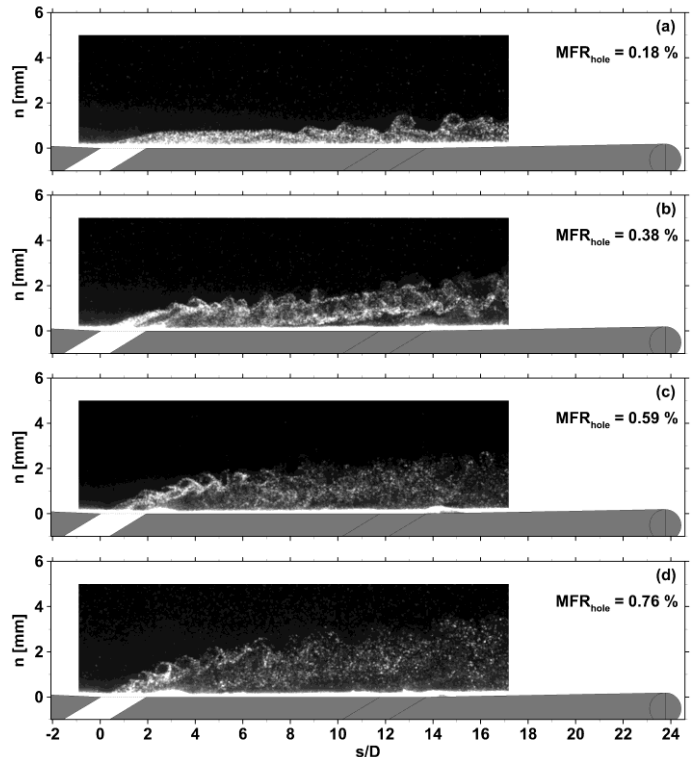


**Fig. 10: Instantaneous visualizations of Row #1 cooling jet (hole centreline).**

dominant coherent vortical structures for an inclined film cooling jet that stays attached to the vane surface, at  $VR$  lower than 1.

Consistently with the effectiveness data reported in Fig. 7 for  $MFR_{hole} = 0.22\%$ , the jet dynamics for a  $MFR_{hole}$  of about 0.18% is able to guarantee an effective film cooling coverage over a wide extension of the vane surface downstream of the hole.

Pictures of the coolant jets when the  $MFR_{hole}$  is increased above 0.38% are provided in Figs. 10b-d. A first major difference with respect to the previous  $MFR_{hole} = 0.18\%$  case is the appearance of counter-clockwise vortical structures due to the breakdown of the Kelvin Helmholtz instability of the shear layers, in agreement with Fawcett et al. (2010). This is consistent with the comments above about the overspeed in the streamwise velocity profiles (Fig. 9a). Moreover, these vortices arise more and more upstream as  $MFR$  is increased, with a consequent increasing mixing and faster spread of the jet, as already observed when commenting the rms velocity components profiles of Figs. 9b,c.

For the  $MFR_{hole} = 0.76\%$  case the shear layer vortices are quite well defined and the high speed flow visualizations allowed to estimate their shedding frequency. Several sequences of images have been recorded by adjusting the time interval between two exposures. A shedding frequency equal to  $f = 1/\Delta t = 42 \pm 2$  kHz has been determined by selecting the time interval  $\Delta t$  that produces the best superimposition between successive coherent structures. On the basis of the hole diameter  $D$  and the coolant velocity  $U_c$ , the value of which can be extrapolated from the  $VR$  data of Fig. 6, a Strouhal number is defined as  $St = f \cdot D / U_c$ . Due to the uncertainty in the evaluation of the  $VR$  previously commented, two values of  $St$  number have been computed:  $1.19 \pm 0.05$ , if  $VR$  defined on the mass averaged coolant velocity is used, and  $1.09 \pm 0.05$ , if  $VR$  based on the jet velocity peak is considered. Although the present uncertainty in the  $VR$ , both values are in good agreement with the results of Fawcett et al. (2011), that reported Strouhal numbers in the range 1.0-1.2.

Finally, if Figs. 10c,d at  $MFR_{hole} = 0.59\%$  and 0.76% are compared with Fig. 10b at  $MFR_{hole} = 0.38\%$ , the jet axis turns out to be more inclined with respect to the wall, therefore supporting the previous hypothesis of jet lift-off. Therefore, the observed coolant jet dynamics at  $MFR_{hole}$  above 0.59% is consistent with the loss of thermal protection shown in Fig. 7. However, the case at  $MFR_{hole} = 0.38\%$  appears to be an intermediate condition that unfortunately is not supported at the present time by thermal data.

### Second cooling row (Row #2).

The LDV results for the second row of cooling holes are provided in Fig. 11. The streamwise velocity profiles (Fig. 11a) are characterized by the absence ( $MFR_{hole} = 0.27\%$  and 0.53%) or the presence of a weak ( $MFR_{hole} = 0.68\%$ ) overspeed. Only for  $MFR_{hole} = 0.87\%$  a velocity peak of  $1.25 U_e$  is reached, which is always lower than the values measured for the first row. Indeed, a similar overspeed value is obtained in the first row at  $MFR_{hole} = 0.53\%$ . Therefore, it can be concluded that the  $VR$  for row #2 jets is always lower than the one of row #1 at constant  $MFR$ . This also explains the lower turbulent activity that is measured for the downstream jets (Figs. 11b-d). In particular, the shear stresses are always very weak and hardly detectable (Fig. 11d) and the streamwise (Fig. 11b) and wall normal (Fig. 11c) fluctuations have lower peak values that are localized closer to the vane surface. This is particularly evident for  $MFR_{hole} = 0.59\%$  and 0.76% conditions. Moreover, it can be observed that the fluctuation values at high elevation from the wall ( $n > 1.2$  mm) are always increasing with  $MFR$  and do not converge to a unique value as it occurred for row #1. This effect, which is slightly detectable also in the  $U$  velocity profiles, is due to the strong and rapid diffusion of the jets coming from row #1 that occurs as soon as  $MFR_{hole}$  reaches value of 0.68%. A proof of this behavior is provided in Figs. 12c,d where the flow visualizations clearly show flow tracers coming from upstream, indicating the existence of a strong vertical penetration of the first row of cooling jets.

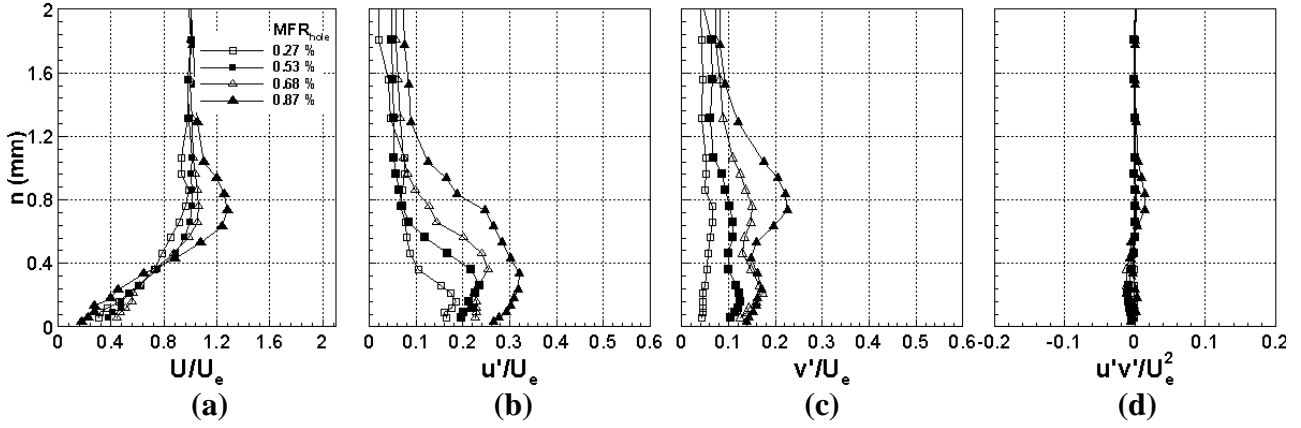


**Fig. 11: Row #2 boundary layer profiles ( $s/D = 14.5$  - hole centreline).**

For blowing conditions at  $MFR_{hole}$  of 0.18% and 0.38%, the flow visualizations of Figs. 12a,b show thin layers of coolant always attached to the vane surface. Even if the coolant traces appear as non uniform with periodical perturbations, no clear traces of coherent vortical structures can be reported. The present coolant jet dynamics is again consistent with the active thermal protection actually measured downstream of row #2 (see the film cooling effectiveness distribution in Fig. 7). Only for the largest  $MFR$  value a trace of counter-clockwise vortices can be found, coherently with the local overspeed previously commented (Fig 11a). However a shedding frequency could not be determined since the structures appear less defined than for row #1 and because of a lower image contrast (due to the flow tracers coming from the upstream holes).

The commented changes in the jet dynamic behavior is finally responsible for the decay of the thermal effectiveness values found for the highest blowing conditions here considered (Fig. 7). As a final remark, it can be commented how the thermal protection persists at non negligible values also at the highest  $MFR$  in view of the lower turbulent activity and mixing that characterize the second row of jets and that are favored by the strong acceleration of the main stream.

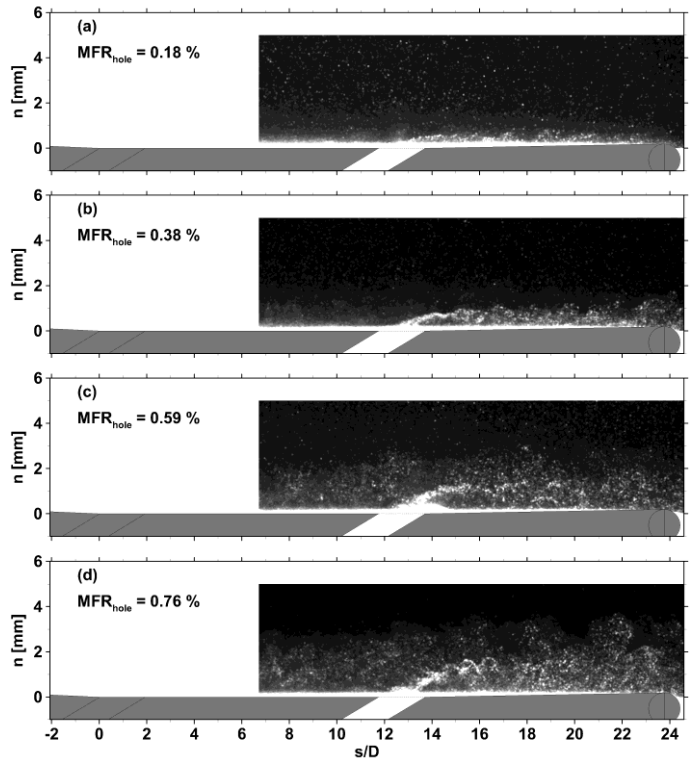


**Fig. 12: Instantaneous visualizations of Row #2 cooling jet (hole centreline).**

## CONCLUSIONS

A detailed characterization of a nozzle vane cascade with cooled rear pressure side was carried out at a low isentropic Mach number of 0.2 with varying holes coolant mass flow ratio up to about 0.9% on a large scale model. Detailed LDV data about both mean and fluctuating velocity components for variable injection conditions allowed to describe the mixing process in the near hole exit region, supporting the thermal behaviour of cooling jets. These data showed the presence of an uneven sharing between injection rows, with row #1 providing a higher coolant discharge than row #2. This in turn resulted in higher velocity ratios and increased turbulence characteristics,

responsible for the quick decay in thermal protection capability of row #1. Lower VR values and reduced turbulence levels were instead observed downstream of row #2, according with the higher thermal protection reached even at high injection rates. In any case, a certain degree of anisotropy characterises the turbulence characteristics. The LDV based quantitative analysis was finally supported by flow visualizations that confirmed the presence of hairpin vortices at low injection rates, at least downstream of row #1, and of counter clockwise rotating shear layer vortices at higher injection ratios, especially when the jets lift-off from the wall.

## ACKNOWLEDGEMENTS

The authors are indebted to Prof. A. Perdichizzi for his invaluable support.

## REFERENCES

- Barigozzi G., Franchini G., Perdichizzi A. (2003) *Blowing Rate and Inlet Turbulence Intensity Effects on the Aerodynamic Performance of a Film Cooled Nozzle Vane Cascade*, in Proceedings of the 5<sup>th</sup> European Conference on Turbomachinery Fluid Dynamics and Thermodynamics, Praha.
- Barigozzi G., Ravelli S., Perdichizzi A. (2012) *Pressure Side and Cutback Trailing Edge Film Cooling in a Linear Nozzle Vane Cascade at Different Mach Numbers*, ASME J Turbomachinery, 134, 051037-1:10.
- Barigozzi G., Armellini, A., Mucignat, C., Casarsa, L. (2012) *Experimental Investigation of the Effects of Blowing Conditions and Mach number on the Unsteady Behavior of Coolant Ejection through a Trailing Edge Cutback*, Int. J. Heat and Fluid Flow, 37, 37-50.
- Fawcett, R.J., Wheeler, A.P.S., He, L., Taylor, R. (2010) *Experimental Investigation into Unsteady Effects on Film Cooling*, In Proceedings of the ASME Turbo Expo, Glasgow, GT2010-22603.
- Fawcett, R.J., Wheeler, A.P.S., He, L., Taylor, R. (2011) *Experimental Investigation into the Impact of Crossflow on the Coherent Unsteadiness within Film Cooling Flows*, In Proceedings of the ASME Turbo Expo, Vancouver, GT2011-45376.
- Han, J.-C., Dutta, S. and Ekkad, S.V. (2000) *Gas Turbine Heat Transfer and Cooling Technology*, Taylor & Francis, New York.
- Karpuk M.E., Tiederman, W.G. (1976) *Effect of Finite-Size Probe Volume upon Laser Doppler Anemometer Measurements*, AIAA Journal, 14 (8), 1099-1105.
- Pietrzyk J.R., Bogard D.G., Crawford, M.E. (1989) *Hydrodynamics Measurements of Jets in Crossflow for Gas Turbine Film Cooling Application*, ASME J Turbomachinery, 111, 139-145.
- Pietrzyk J.R., Bogard D.G., Crawford, M.E. (1990) *Effects of Density Ratio on the Hydrodynamics of Film Cooling*, ASME J Turbomachinery, 112, 437-443.
- Puddu P., Cambuli F., Paderi M., Ghiani M., (2011) *Measurements and Numerical Simulations in a Gas Turbine Cascade with Curback Blade Trailing Edge*, Proc. of the 10<sup>th</sup> International Symposium on Experimental and Computational Aerothermodynamics of Internal Flows, ISAI10-172.
- Roy, S., Kapadia, S., Heidmann, J.D. (2003) *Film Cooling Analysis Using DES Turbulence Model*, In Proceedings of the ASME Turbo Expo, Atlanta, GT-2003-38140.
- Sinha, A.K., Bogard D.G., Crawford, M.E. (1991) *Gas Turbine Film Cooling: Flowfield due to a Second Row of Holes*, ASME J Turbomachinery, 113, 450-456.
- Thole, K., Gritsch, M., Schulz, A., Wittig, S. (1996) *Flowfield Measurements for Film-Cooling Holes with Expanded Exits*, ASME J Turbomachinery, 120, 327-336.
- Tyagi M. and Acharya, S. (2003) *Large Eddie Simulation of Film Cooling Flow from an Inclined Cylindrical Jet*, ASME J Turbomachinery, 125, 734-742.